FEBS Letters

FEBS PRESS science publishing by scientists

# Localization of the ubiquitin ligase Dma1 to the fission yeast contractile ring is modulated by phosphorylation

Jun-Song Chen, Christine M. Jones*, Maya G. Igarashi, Liping Ren, Alyssa E. Johnson[$] and Kathleen L. Gould

Department of Cell and Developmental Biology, Vanderbilt University School of Medicine, Nashville, TN, USA

**Correspondence**
K. L. Gould, Department of Cell and Developmental Biology, Vanderbilt University School of Medicine, PMB 407935, 485 21st Ave S. Nashville, TN 37240-7935, USA
Tel: +1 615 343-9502
E-mail: kathy.gould@vanderbilt.edu

**Present address**
*Arvinas Inc., 5 Science Park, New Haven, CT 06511, USA
[$]Department of Biological Sciences, Louisiana State University, Baton Rouge, LA 70803, USA

(Received 6 September 2021, revised 13 October 2021, accepted 14 October 2021, available online 2 November 2021)

doi:10.1002/1873-3468.14211

Edited by Ivan Sadowski

**The timing of cytokinesis relative to other mitotic events in the fission yeast *Schizosaccharomyces pombe* is controlled by the septation initiation network (SIN). During a mitotic checkpoint, the SIN is inhibited by the E3 ubiquitin ligase Dma1 to prevent chromosome mis-segregation. Dma1 dynamically localizes to spindle pole bodies (SPBs) and the contractile ring (CR) during mitosis, though its role at the CR is unknown. Here, we examined whether Dma1 phosphorylation affects its localization or function. We found that preventing Dma1 phosphorylation by substituting the six phosphosites with alanines diminished its CR localization but did not affect its mitotic checkpoint function. These studies reinforce the conclusion that Dma1 localization to the SPB is key to its role in the mitotic checkpoint.**

**Keywords:** cytokinesis; fission yeast; protein kinase; septation initiation network; signaling; spindle pole body; ubiquitin ligase

The accurate division of a cell into two daughter cells with identical complements of genomic material is essential, as failure to do so can result in aneuploidy or cell death. In the fission yeast *Schizosaccharomyces pombe*, the proper coordination of mitotic exit with cytokinesis is determined by the septation initiation network (SIN), a protein kinase cascade that normally initiates cytokinesis only after chromosome segregation is complete (for reviews see [1–3]). When the mitotic spindle cannot form, the SIN is inhibited to prevent cytokinesis from occurring before chromosomes have safely segregated [4,5]. SIN inhibition during a mitotic error relies on the dimeric E3 ubiquitin ligase Dma1 [5–8], a member of the forkhead-associated (FHA) and RING finger (RF) family [9].

Dma1 has a very complex localization pattern during the cell cycle. It dynamically localizes to spindle pole bodies (SPB) during mitosis [5,10] and ubiquitinates the SIN scaffold protein Sid4 that is detected exclusively at SPBs [6,11]. Dma1 binding and ubiquitination of Sid4 requires casein kinase 1 (CK1)-

**Abbreviations**
5-FOA, 5-Fluoroorotic Acid; CK1, casein kinase 1; CR, contractile ring or cytokinetic ring; DTT, dithiothreitol; FHA, forkhead-associated; HBH, hexahistidine biotin hexahistidine; HU, hydroxyurea; LC-MS, liquid chromatography mass spectrometry; MBP, maltose-binding protein; mNG, mNeonGreen; NP-40, Nonidet P40; ORF, open reading frame; PMP, protein metallophosphatase; PVDF, polyvinylidene difluoride; RF, ring finger; RING, really interesting new gene; ROI, region of interest; *S. pombe*, *Schizosaccharomyces pombe*; SEM, standard error of the mean; SIN, septation initiation network; SPB, spindle pole body; TAP, tandem-affinity purification; YE, yeast extract.

mediated Sid4 phosphorylation, which provides a docking site for Dma1's FHA domain [12]. Sid4 ubiquitination then antagonizes the SPB localization of the Polo-like kinase Plo1 [5,6], the major SIN activator [13–15] so that SIN signaling is inhibited and cytokinesis is delayed. Dma1 also localizes to the site of cell division through an unknown mechanism and for an unknown purpose, first in precursor nodes that eventually form the cytokinetic ring (CR) [16], then to the CR; Dma1 leaves the site of division transiently during late anaphase, only to return prior to cell division [10]. Dma1 overproduction or tethering Dma1 to SPBs blocks SIN activity and results in cell death [5,10,17], indicating its levels, localization, and activity must be properly regulated.

We previously determined that Dma1 auto-ubiquitination influences its SPB localization and function in the mitotic checkpoint. Specifically, Dma1 auto-ubiquitination prevents its binding to Sid4 and therefore Dma1 auto-ubiquitination is implicated in checkpoint silencing [10]. Here, we investigated potential regulation of Dma1 by phosphorylation. We found that Dma1 is phosphorylated in vivo throughout the cell cycle, and we identified six phosphorylated residues scattered throughout the protein. Four of the six sites can be targeted by a combination of three master kinases *in vitro*—Cdk1, Plo1, and CK2, but we obtained no evidence that they control Dma1 phosphorylation *in vivo*. Strikingly, neither phospho-ablating nor phospho-mimicking mutations at any or all of the six sites abolished Dma1 catalytic activity toward itself in vitro or its checkpoint substrate Sid4, as demonstrated by Sid4's continued ubiquitination in phosphomutant strains. While we found that loss of phosphorylation altered Dma1's localization to the CR in early mitosis, we did not detect an impact of phosphorylation on Dma1 localization to SPBs or its function in delaying cytokinesis during a mitotic arrest. Our results reinforce the conclusion that Dma1's function in the mitotic checkpoint depends solely on its SPB localization.

## Materials and methods

### Yeast methods

Yeast strains were grown in yeast extract (YE) with appropriate supplements [18]. Genes were tagged endogenously at the 3′ end of their open reading frame (ORF) with *FLAG$_3$:kan$^R$*, *GFP:kan$^R$*, *HA$_3$-TAP:kan$^R$*, *mNeonGreen:kan$^R$*, *mCherry:-nat$^R$*, or *HBH:kan$^R$* using pFA6 cassettes as previously described [19,20]. For *dma1* gene replacements, *dma1::ura4+* was transformed with the appropriate pIRT2–*dma1* mutant. Stable integrants were selected by resistance to 1.5 mg·mL$^{-1}$ 5-FOA. Mutants were identified by colony PCR with primers inside and outside of the 3′-flanking regions, and validated through DNA sequencing of the entire ORF.

For blocking *nda3-KM311* strains in prometaphase, cultures were grown at the permissive temperature (32 °C) and then shifted to the restrictive temperature (18 °C) for 5.5 or 6 h. For quantitative imaging, cells were fixed for 10 min with 70% ethanol and washed with PBS. For blocking *cdc10-V50*, *cdc25-22*, and *mts3-1* strains, cultures were grown at the permissive temperature (25 °C) and then shifted to the restrictive temperature (36 °C) for 3.5 h. For blocking strains with hydroxyurea (HU) in Fig. 1, cultures were grown at 25 °C, treated with a final concentration of 12 mM HU for 3 h and then dosed again with a final concentration of 6 mM HU for an additional 2 h.

### Molecular biology methods

Plasmids were generated by standard molecular biology techniques. *dma1* mutations were made either in the context of a gene fragment in the pIRT2 vector that included 500 bp upstream and downstream of the ORF or in the context of the ORF in pMAL2-c (New England Biolabs, Ipswich, MA, USA) or pET-His6-MBP preScission LIC cloning vector (HMPKS; Addgene plasmid # 29721) using a QuikChange site-directed mutagenesis kit (Agilent Technologies, Santa Clara, CA, USA). In *dma1-6A*, the mutations are: S4A, T18A, S20A, S166A, S251A, and S266A; in *dma1-6D/E*, the mutations are: S4D, T18E, S20D, S166D, S251D, and S266D.

### *S. pombe* protein methods

Cell pellets were washed once in NP-40 buffer (10 mM sodium phosphate pH 7.0, 1% Nonidet P40, 150 mM NaCl, 2 mM EDTA) with inhibitors (1.3 mM benzamidine, 1 mM PMSF, and 1 Complete Protease Inhibitor Cocktail Tablet, EDTA-free per 50 mL) and lysed by bead disruption. For denaturing lysis, 500 µL SDS lysis buffer (10 mM sodium phosphate pH 7.0, 1% SDS, 1 mM DTT, 1 mM EDTA, 50 mM NaF, 100 µM sodium orthovanadate, 1 mM PMSF, and 4 µg·mL$^{-1}$ leupeptin) was added and samples were incubated at 95 °C for 2 min, lysate was extracted with 800 µL NP-40 buffer and transferred to a fresh eppendorf tube. For native lysis, the lysate was extracted with 500 µL NP-40 buffer and again with 800 µL, then transferred to a fresh eppendorf tube. Extractions were followed by a 10 min clearing spin.

Proteins were immunoprecipitated from protein lysates using an excess of antibody (listed below) and rotating at 4 °C for 1 h, followed by addition of Protein A or G Sepharose beads (GE Healthcare, Boston, MA, USA), as appropriate, and mixing at 4 °C for 30 min. Samples were washed four times with NP-40 buffer. Antibodies: 4 µL of

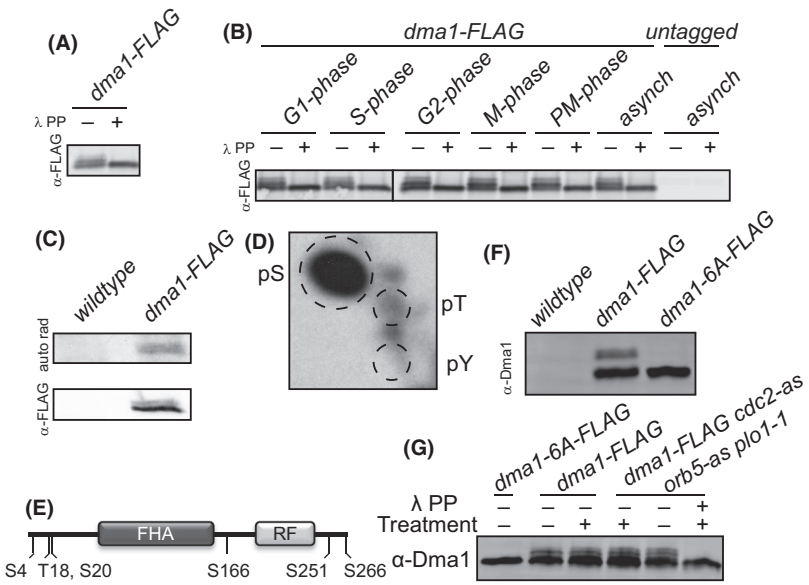


**Fig. 1.** Dma1 is phosphorylated through the cell cycle. (A-B) Immunoblot analysis of Dma1-FLAG immunoprecipitates, treated (+) or not (–) with lambda phosphatase, from asynchronously growing cells (A) or cells arrested at a variety of cell cycle stages (G1 phase, *cdc10-V50*; S phase, HU; G2 phase, *cdc25-22*; metaphase, *mts3-1*; and prometaphase, *nda3-KM311*) (B). (C) Autoradiography and immunoblot analysis of Dma1-FLAG immunoprecipitates from the indicated strains that were labeled *in vivo* with $^{32}$P-orthophosphate. (D) Phosphoamino acid analysis of wild-type Dma1 from C. The positions of phosphoserine, phosphothreonine, and phosphotyrosine standards are indicated with dotted circles. (E) Schematic of Dma1 with phosphorylation sites identified by LC-MS/MS indicated. FHA, Forkhead-associated domain; RF, Ring Finger domain. (F) Immunoblot analysis of Dma1-FLAG immunoprecipitates from the indicated strains resolved on a PhosTag gel. (G) Immunoblot analysis of Dma1-FLAG immunoprecipitates from the indicated strains resolved on a PhosTag gel. "Treatment" denotes shifting cells from 25 °C to 36 °C for 1.5 h followed by adding 10 μM 1-NMPP1 and 30 μM 3-BrBPP1 for 15 min.

1 μg·μL$^{-1}$ anti-GFP (IC9H4, a mouse monoclonal antibody produced in the Vanderbilt antibody and protein resource core), 2 μL of 1 μg·μL$^{-1}$ anti-FLAG (Sigma-Aldrich, St. Louis, MO, USA), or 3 μL rabbit anti-Sid4 antiserum (VU364) [12]. For phosphatase treatment, immunoprecipitated protein was washed twice with 25 mM HEPES-NaOH (pH 7.4) and 150 mM NaCl, then treated with lambda phosphatase (New England Biolabs) in 1× NEBuffer for protein metallophosphatase (PMP) and 1 mM $MnCl_2$ and incubated at 30 °C for 30–60 min with agitation.

Proteins were resolved by PAGE (see below), transferred by electroblotting to a polyvinylidene difluoride (PVDF) membrane (Immobilon FL; Millipore, Bedford, MA, USA), blocked with Odyssey Blocking Buffer (LI-COR Biosciences, Lincoln, NE, USA), and incubated with primary antibodies at the following concentrations/dilutions: 1 : 10 000 anti-Cdc2 (anti-PSTAIR, Sigma-Aldrich), 0.4 μg·mL$^{-1}$ anti-GFP (Roche, Basel, Switzerland), 1 μg·mL$^{-1}$ anti-FLAG (Sigma-Aldrich), 1 : 2000 anti-Sid4 serum, or 1 : 5000 anti-Dma1 serum (VU377) [10] overnight at 4 °C. Primary antibodies were detected with secondary antibodies coupled to IRDye680 or IRDye800 (LI-COR Biosciences, Lincoln, NE, USA) and visualized using an Odyssey Infrared Imaging System (LI-COR Biosciences). Resolving gels: 3%–8% Tris-acetate PAGE used for Dma1-FLAG blotting except for a 10% SDS/PAGE containing 25 μM PhosTag in Fig. 1F,G; 4%–12% NuPAGE used for Sid4 and Dma1 ubiquitination assay blotting, 12% Tris-glycine PAGE used for Cdc2 blotting, 10% Tris-glycine PAGE used for MBP-Dma1 blotting.

## Protein expression and purification

For phosphorylation of Dma1 variants shown in Fig. S2A, the variant cDNAs were cloned into pMAL-2c and then transformed into *Escherichia coli* Rosetta2(DE3)pLysS cells. Maltose-binding protein (MBP)-Dma1 fusions were induced by addition of 0.8 mM IPTG and overnight incubation at 18 °C. Bacterial cells were lysed by incubating with 300 μg·mL$^{-1}$ lysozyme for 20 min followed by sonication. Proteins were affinity purified on amylose resin (NEB E8021) in MBP column buffer (100 mM NaCl, 20 mM Tris-HCl, 1 mM EDTA, 1 mM DTT, and 1% Nonidet P40). Resin was washed with MBP column buffer and protein was eluted with MBP column buffer containing 10 mM maltose.

For all other experiments, *dma1* variants were cloned into pET-His$_6$-MBP preScission LIC cloning vector. Proteins were induced in *E. coli* Rosetta2(DE3)pLysS cells by addition of 0.4 mM IPTG and overnight incubation at 18 °C. Cells were lysed using 300 μg·mL$^{-1}$ lysozyme for 20 min followed by sonication. Proteins were affinity purified

on pre-washed amylose resin (New England Biolabs) in MBP column buffer (100 mM NaCl, 20 mM Tris-HCl pH 7.4 mM EDTA, 1 mM DTT, and 1% Nonidet P40). Dma1 was cleaved from MBP by adding 1 μL (2 units) of PreScission protease to ~500 μg MBP-Dma1 on amylose beads (in 200 μL MBP column buffer) and incubating at 4 °C overnight. The supernatant containing cleaved Dma1 was retrieved and the concentration of Dma1 was determined by SDS/PAGE using BSA as standard.

### *In vitro* ubiquitination assay

Ubiquitination reactions included 0.2 μg recombinant Dma1 cleaved from MBP, 175 nM E1 (recombinant human His6-UBE1, R&D Systems), 0.19 μM E2 (recombinant human UbcH5α/UBE2D1, R&D Systems, Minneapolis, MN, USA), 100 $\mu g \cdot mL^{-1}$ methylated ubiquitin, 5 mM ATP, and 1x ubiquitination buffer (50 mM Tris-HCl pH 7.5, 2.5 mM $MgCl_2$, 0.5 mM DTT). These 20 μL reactions were incubated with agitation at 30 °C for 120 min before adding SDS sample buffer. Ubiquitination products and Dma1 were detected by immunoblotting with a 1 : 15 000 dilution of anti-Dma1 serum [10].

For ubiquitination assays of immunoprecipitated Dma1-GFP, the mock or λ-phosphatase-treated immunoprecipitates were washed twice with ubiquitylation buffer before being combined in 20 μL ubiquitylation reactions as above. Reactions were incubated with agitation at 30 °C for 90 min before adding SDS sample buffer to quench the reaction. To assess the extent of Dma1's ubiquitin modification, proteins were separated by SDS/PAGE and detected by immunoblotting with anti-GFP antibody and/or anti-Dma1 serum.

To determine abundances of Dma1 in immunoblotting experiments, signal intensities within identical squares or rectangles drawn around single or multiple bands were quantified using an Odyssey instrument. Experiments were performed twice.

### Protein purification and mass spectrometry

Endogenously tagged versions of Dma1 (Dma1-TAP and Dma1-HBH) were purified as previously described [21–23] and analyzed by 2D-LC-MS/MS as previously described [24,25]. RAW files were processed using two pipelines: (a) using Myrimatch (v 2.1.132) [26] and IDPicker (v 2.6.271.0) [27] as previously described [28] and (b) using TurboSEQUEST, Scaffold (v 4.4.7) and Scaffold PTM (v 3.0.0) as previously described [29].

### *In vivo* radio-labeling

Ten milliliters of *S. pombe* cells were grown in reduced (20 mM $NaH_2PO_4$) phosphate minimal media supplemented with the appropriate amino acids to mid-log phase. Cells were labeled with 5 mCi $^{32}$P-orthophosphate for 4 h at 36 °C. Denatured cell lysates were prepared and Dma1-FLAG was immunoprecipitated with anti-FLAG. Immunoprecipitates were resolved on a 6%–20% gradient SDS polyacrylamide gel, transferred to a PVDF membrane and phosphorylated proteins were detected by autoradiography for 4 days at −80 °C with intensifying screen. The membrane was then immunoblotted for anti-FLAG. $^{32}$-P-labeled Dma1 was subjected to partial acid hydrolysis while bound to the PVDF membrane [30], and the phosphoamino acids were separated in two dimensions by thin-layer electrophoresis at pH 1.9 and 3.5 [31].

### *In vitro* kinase assays

Kinase reactions were performed in protein kinase buffer (10 mM Tris, pH 7.4, 10 mM $MgCl_2$, and 1 mM DTT- or NEB-supplied buffer) with 5 μM cold ATP, 3 μCi of γ-$^{32}$P-ATP, and recombinant CK2 (New England Biolabs), insect cell-produced Cdc2-Cdc13 or insect cell-produced Plo1 at 30 °C for 30 min. Reactions were quenched by the addition of SDS sample buffer. Proteins were separated by SDS–PAGE and detected by Coomassie Blue (Sigma) staining or transferred to polyvinylidene fluoride (PVDF) membrane for detection by autoradiography.

### Microscopy methods

Images of *S. pombe* cells were acquired using a Personal DeltaVision microscope system (Cytiva Life Sciences, Marlborough, MA, USA), which includes an Olympus IX71 microscope, 60×NA 1.42 Plan Apochromat and 100×NA 1.40 U Plan S Apochromat objectives, live-cell and standard filter wheel sets, a pco.edge 4.2 sCMOS camera, and SoftWoRx imaging software (Applied Precision, Inc., Issaquah, WA, USA). Images were acquired at 25 °C. All images were deconvolved with 10 iterations except for the images used for fluorescence quantification. Time-lapse imaging was performed using a CellASIC ONIX microfluidics perfusion system (Millipore Sigma, Burlington, MA, USA). Cells were loaded into Y04C plates for 5 s at 8 psi, and YE liquid medium flowed into the chamber at 5 psi throughout imaging. For all images, *Z*-series optical sections were taken at 0.5 μm spacing and images were acquired every 2 min. All images for quantification were sum projected. Images in figures were deconvolved and max projected.

In Fig. S3, the events were defined as follows: "Arrival at division site" was the first frame in which Dma1-mNG was detected at division site. "Ring formation" was the first frame where a coherent ring was visible. "SPB blinks" was the first frame where Dma1-mNG leaves or dims at one or both SPBs. "Anaphase B begins" was the first frame where the SPBs move toward the cell poles as the spindle elongates. "Disappearance from division site" was the frame where Dma1-mNG no longer detected at the division site.

"Spindle full length" was the frame where the SPBs are furthest apart during mitosis. "Re-appearance at division site" was the first frame in which Dma1-mNG returns to the division site.

Fluorescence intensity measurements were made with ImageJ software (National Institutes of Health, Bethesda, MD, USA). All intensity measurements were corrected for background. In each image used, background measurements were taken from an area without any cells. The intensity of the background was divided by the area to give the average intensity per pixel of the background. This was then multiplied by the area of the region of interest (ROI) used to measure fluorescence intensity and subtracted from that ROI's raw intensity measurement to get the final intensity measurement corrected for background. For whole cell fluorescence measurements, the corrected intensity measurements were divided by the area of the ROI. For SPB intensity measurements, both Dma1-mNG and Sad1-mCherry SPBs were corrected for background. Additionally, Dma1-mNG SPB intensity was divided by the Sad1-mCherry measurement of the same SPB. In Fig. 3D, constricted *rlc1-mCherry* was used to indicate cells with a septum for quantification. In Fig. 3E, *sad1-mCherry* and *rlc1-mCherry* were used to indicate cells at the end of anaphase B for quantification. For Fig. 3F, unconstricted *rlc1-mCherry* was used to indicate early mitotic CRs for quantification.

### Checkpoint assay

Log phase cells growing in YE at 32 °C were synchronized in S-phase by the addition of 12 mM hydroxyurea (Sigma) for 3 h. The arrested cells were then filtered, washed with YE media to remove hydroxyurea while on the filter, and immediately incubated in pre-cooled YE media at 19 °C. Septation indices were measured periodically (every 30 min or 1 h) for up to 12 h by counting live cells under a phase contrast microscope.

### Quantification and statistical analysis

Calculations of mean, standard error of the mean (SEM), and statistical significances were performed with Prism 8.0 (GraphPad Software, San Diego, CA, USA). Significance was defined by a $P$ value $\leq 0.05$. One-way ANOVA was used with Tukey's post hoc test for multiple comparisons.

## Results

### Dma1 is phosphorylated throughout the cell cycle

Dma1 SPB localization and Dma1-mediated ubiquitination of Sid4 are cell cycle dependent [6,10], leading us to explore the molecular mechanisms that regulate Dma1 activity. Because phosphorylation provides a rapid and reversible means of regulating protein function often coupled to ubiquitination [32–34], we examined whether Dma1 is phosphorylated *in vivo*. Using immunoblot analysis of Dma1 immunoprecipitates, treated with or without λ phosphatase, we detected Dma1 phosphorylation in asynchronous cells that could be observed by slower migration in SDS/PAGE (Fig. 1A). Further examination of Dma1 in various cell cycle arrests showed that Dma1 phosphorylation occurs throughout the cell cycle (Fig. 1B). *In vivo* labeling with $^{32}$P-orthophosphate followed by immunoprecipitation and phosphoamino acid analysis showed that the majority of Dma1 phosphorylation occurred on serine residues (Fig. 1C,D).

### Identification of Dma1 phosphorylation sites

To determine the sites of Dma1 phosphorylation, we performed liquid chromatography mass spectrometry (LC-MS)/MS analysis on Dma1 purified from *S. pombe* cells using a variety of epitope tags, lysis procedures, and cell cycle blocks. In all, six sites were identified: 1 threonine and 5 serines (Figs 1E and S1). Four of these sites (S4, T18, S251, S266) were also identified in global phosphoproteomic screens [35–37]. To investigate if this cohort of six was the full complement of Dma1 phosphorylation sites, we replaced *dma1*$^{+}$ with a mutant version in which all six sites were replaced with alanines. While multiple species of Dma1 were detected on a PhosTag-containing gel, Dma1-6A co-migrated with the fastest migrating band (Fig. 1F), indicating the absence of phosphorylation.

### Dma1 is phosphorylated *in vitro* by several master kinases

Examination of the linear sequences surrounding the six identified phosphosites showed that four fit known kinase consensus sequences; S166 fits the Cdk1 consensus [38,39], S251 fits the Plo1 consensus [40], and T18 and S20 fit the CK2 consensus [41,42]. To determine if Cdk1, Plo1, and CK2 were indeed capable of phosphorylating Dma1, *in vitro* kinase assays were performed with recombinant Dma1 and commercially available or insect cell-produced kinases (Fig. S2). Cdk1 phosphorylation of MBP-Dma1-S166A was diminished relative to MBP-Dma1 (Fig. S2A). Similarly, Plo1 could not phosphorylate MBP-Dma1-S251A (Fig. S2B). It is notable that S251 but not S166 was found to be specifically present during mitosis in two phosphoproteomic screens [35,36]. Lastly, CK2 phosphorylation of MBP-Dma1 was diminished with

the MBP-Dma1-T18A S20A mutant and lost with the MBP-Dma1-T18A S20A S266A mutant (Fig. S2C), indicating that CK2 phosphorylation can occur not only at the predicted T18 and S20 sites but also at the previously unassigned S266 site. The S4 phosphorylation site does not fit a known kinase consensus sequence and it is not phosphorylated in vitro by Cdk1, Plo1, or CK2.

To determine whether these three kinases were involved in Dma1 phosphorylation *in vivo*, we combined analog-sensitive (*cdc2-as, orb5-as*) and temperature-sensitive (*plo1-1*) alleles. Despite these kinases targeting Dma1 *in vitro*, we found no evidence that inhibiting any of them singly (not shown) or together (Fig. 1G) changed Dma1 phosphostatus as monitored by SDS/PAGE mobility suggesting that these kinases are not responsible for regulating Dma1 phosphostatus in cells.

## Dma1 phosphostate does not significantly influence its ubiquitination activity

We next investigated whether phosphorylation modulates Dma1 ubiquitination activity *in vivo* and *in vitro*. We constructed phospho-ablating and potentially phospho-mimetic *dma1* mutations by replacing the six phosphorylated serine and threonine residues with alanines (*dma1-6A*), or aspartates for serines and glutamate for threonine (*dma1-6D/E*), respectively. These mutant constructs (*dma1-6A* and *dma1-6D/E*) were each integrated at the endogenous *dma1* locus, and we then examined ubiquitination of Dma1's known target, Sid4, in either asynchronously growing or pro-metaphase arrested cells. To distinguish Sid4 ubiquitination from Sid4 phosphorylation, Sid4 immunoprecipitates were treated with λ-phosphatase prior to immunoblotting [12,43]. Although this assay is not quantitative, we found that Sid4 was ubiquitinated to similar levels as in wild-type in both *dma1-6A* and *dma1-6D/E* but was not ubiquitinated in *dma1Δ* (Fig. 2A). This result indicates that the Dma1 phosphomutants are catalytically active toward substrate.

We next examined if phosphorylation affected the ability of Dma1 to auto-ubiquitinate in vitro. Full-length Dma1, which lacks phosphorylation, Dma1-6D/E, and two Dma1 loss-of-function mutants were purified from bacteria as MBP fusions and the MBP moiety was removed prior to auto-ubiquitination assays, which used methylated Ub to prevent chain elongation. The Dma1-I194A mutant that is predicted based on structural modeling to abrogate interaction with cognate E2 enzyme(s) [44] has much reduced E3 activity relative to wild-type *in vivo* and *in vitro* [6,10] (Fig. 2B). Dma1-F233 is a second amino acid within the predicted hydrophobic groove also likely to interact with E2 enzyme(s). As expected, the double mutant Dma1-I194A F233A had even lower levels of auto-ubiquitination activity compared with wild-type (Fig. 2B). Dma1-6D/E auto-ubiquitination was modestly but reproducibly reduced relative to wild-type (Fig. 2B). Specifically, while 82% of wild-type Dma1 became ubiquitinated on at least one site, 71% of Dma1-6D/E did. We also examined the effect of phosphorylation on Dma1 ubiquitination activity by immunoprecipitating Dma1-GFP from prometaphase-arrested cells and then treating the immunoprecipitates with lambda phosphatase or only vehicle prior to an in vitro auto-ubiquitination assay. We found that phosphatase-treated Dma1-GFP auto-ubiquitinated similarly to phosphorylated Dma1-GFP (Fig. 2C). By measuring the amount of ubiquitinated species relative to unmodified Dma1 in each case, we found that there was no significant difference. Taken together, our data suggest that phosphorylation does not play an important role in regulating Dma1 E3 ubiquitin ligase activity.

## A Dma1 phosphomutant has altered intracellular localization

We next tested if Dma1 phosphostatus affected its intracellular localization. Dma1, Dma1-6A and Dma1-6D/E were tagged with mNeonGreen (mNG). The overall levels of the phosphomutants were indistinguishable from wild-type as determined by measuring total fluorescent intensities (Fig. S3A). By live cell imaging, the kinetics of mitotic progression were found to be similar in all three strains (Fig. S3B) and all Dma1 proteins were found to have similar kinetics of cortex, SPB, and CR localization (Figs 3A–C and S3B). Also, all Dma1 variants localized to the site of division and SPBs with similar intensity after spindle breakdown, marked by SPBs starting to move toward each other (Fig. 3D-E). However, we observed that Dma1-6A was significantly more difficult to detect at the first instance of CR localization early in mitosis than either Dma1 or Dma1-6D/E (Fig. 3A–C). We therefore quantified the CR intensities of Dma1 proteins relative to a CR marker, Rlc1-mCherry. We found that indeed, Dma1-6A had significantly reduced CR localization in early mitosis relative to Dma1 and Dma1-6D/E (Fig. 3F).

## Dma1 phosphorylation does not affect its mitotic checkpoint function

Although immunoblotting showed that Sid4 was ubiquitinated in mitotically arrested cells producing any of the Dma1 phosphomutants (Fig. 2A) and Dma1

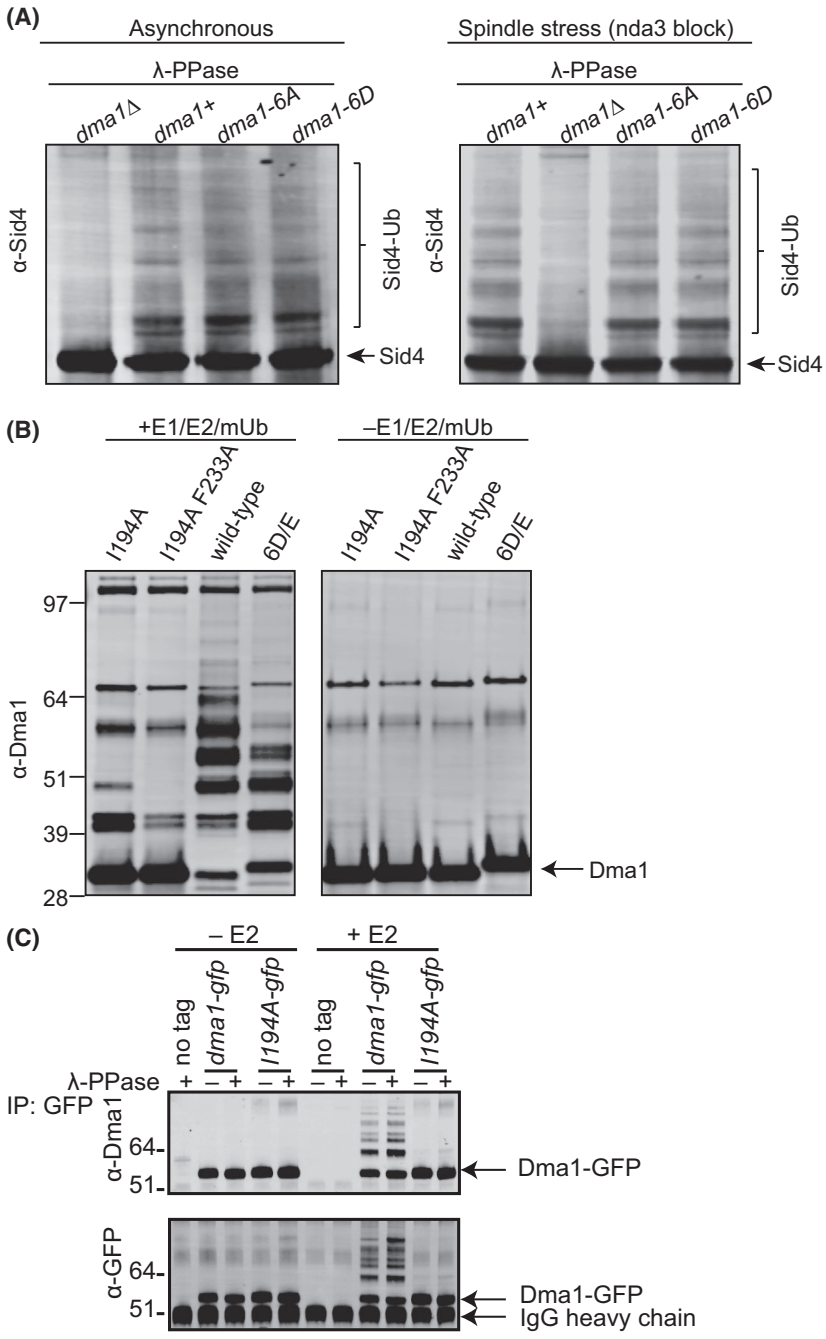


**Fig. 2.** Role of phosphorylation in Dma1 ubiquitination activities. (A) Immunoblot analysis of Sid4 immunoprecipitates treated with phosphatase from asynchronous (left) or *nda3*-arrested (right) cells of the indicated *dma1* genotype. One representative of two separate experiments is shown. (B) Immunoblot analysis of the indicated recombinantly purified and MBP tag-cleaved Dma1 proteins that were incubated with E1 activating enzyme, E2 conjugating enzyme, ATP, and methylated ubiquitin. The Dma1 input prior to the ubiquitination assay is shown (right panel). The percentage of Dma1 auto-ubiquitination was determined by subtracting the amount of unmodified Dma1 (left panels) from the total Dma1 that was added to the reactions (right panels) as determined by quantification on an Odyssey instrument and then dividing ubiquitinated by the total. (C) Immunoblot analysis of the indicated Dma1-GFP immunoprecipitates from prometaphase-arrested cells (*nda3-KM311* cells shifted to 19 °C for 6 h) that were treated with λ-phosphatase or mock-treated followed by incubation with E1 activating enzyme, ATP, methylated ubiquitin, and with (+) or without (–) E2 conjugating enzyme. The ubiquitinated Dma1 species were quantified on an Odyssey instrument and divided by the total amount of Dma1 to determine the percentage of modified Dma1.

phosphomutants appeared to localize normally to SPBs (Fig. 3E), we examined whether the Dma1-dependent checkpoint was fully functional in the *dma1-6A* and *dma1-6D|E* mutants. *dma1*$^{+}$, *dma1-6A*, *dma1-6D|E*, and *dma1*Δ cells that also contained the cold-sensitive *nda3-km311* ß-tubulin mutant and wild-type cells were synchronized in S phase by treatment with hydroxyurea, shifted to 19 °C to induce microtubule depolymerization, and septation kinetics were monitored. We observed that *nda3-km311*, *dma1-6A nda3-km311*, and *dma1-6D|E nda3-km311* cells delayed septation relative to wild-type cells and that *dma1*Δ cells did not (Fig. 4A). These data indicate that Dma1 phosphostate does not significantly influence its function in delaying septation during a mitotic arrest. Consistent with this, we found during a mitotic

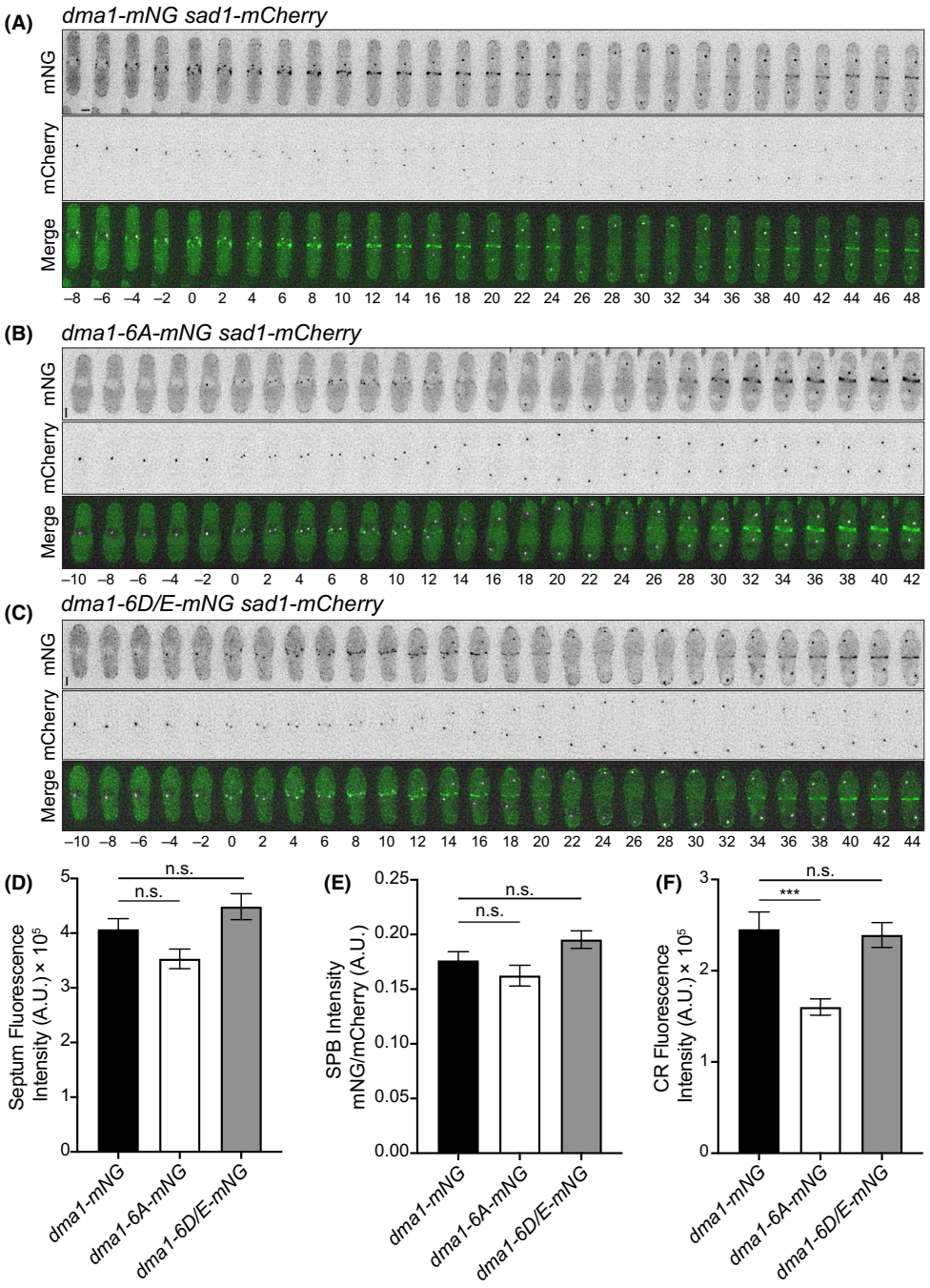


**Fig. 3.** Dma1 phosphomutant localization during cell division. (A–C) Representative montages of live-cell time-lapse imaging of the indicated strains. Images were acquired every 2 min. Time 0 = SPB separation and numbers indicate min from SPB separation. Scale bars, 2 μm. (D–F) Live cell imaging of *dma1-mNG*, *dma1-6A-mNG*, or *dma1-6D/E-mNG* with *rlc1-mCherry* and *sad1-mCherry* and quantification of (D) fluorescence intensity along the septum (when the CR marked by Rlc1-mCherry is fully constricted and a septum is present), (E) SPB intensity at the end of mitosis when two SPBs marked by Sad1-mCherry are well separated and next to the cell tips, or (F) CR fluorescence intensity when a fully formed and unconstricted CR is present. $n \geq 26$ cells. Error bars represent SEM. One-way ANOVA. *** $\leq P = 0.001$. (septum *dma1-mNG vs. dma1-6A-mNG* $P = 0.15$, *dma1-mNG vs. dma1-6D/E-mNG* $P = 0.33$) (SPB *dma1-mNG vs. dma1-6A-mNG* $P = 0.48$, *dma1-mNG vs. dma1-6D/E-mNG* $P = 0.25$; CR *dma1-mNG* vs. *dma1-6D/E-mNG* $P = 0.95$).

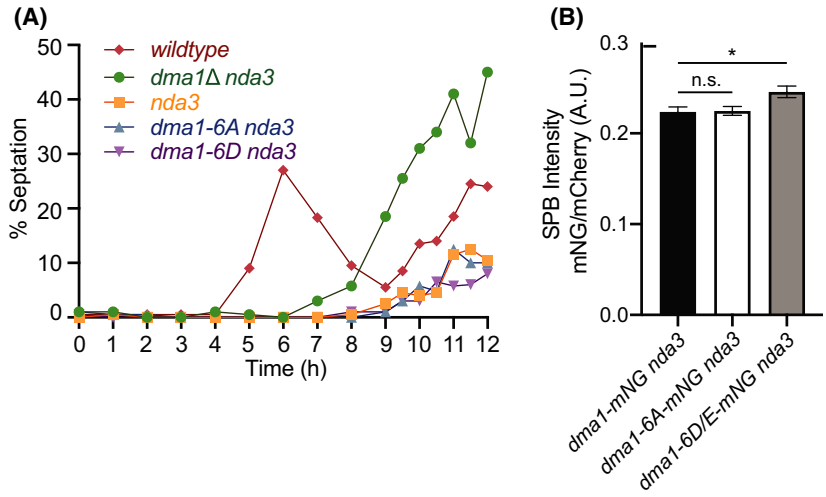


**Fig. 4.** Checkpoint assay. (A) The indicated strains were synchronized in S phase with hydroxyurea and shifted to 19 °C. The septation indices were measured every 1 hour (for early time points) or 30 min (for later time points) for 12 h. One of the two experiments with similar results was shown. (B) Quantification of SPB intensity of arrested and ethanol fixed *dma1-mNG nda3-KM311, dma1-6A-mNG nda3-KM311,* or *dma1-6D/E-mNG nda3-KM311* with *rlc1-mCherry* and *sad1-mCherry*. $n \geq 67$ cells. Error bars represent SEM. One-way ANOVA. $* \leq P$ 0.05 (SPB *dma1-mNG vs. dma1-6D/E-mNG* $P = 0.99$).

checkpoint arrest, the intensities of Dma1 and Dma1 phosphomutants at the SPB relative to the SPB marker, Sad1-mCherry, were very similar (Fig. 4B).

## Discussion

Dma1 signaling must be properly regulated to ensure that its checkpoint activity is quickly activated in the event of a mitotic spindle error and is also reversed when the error is resolved. Here, we tested whether Dma1 phosphostate influences it signaling potential in the mitotic checkpoint that delays cytokinesis until chromosome segregation is complete. We found no evidence that phosphorylation influences Dma1 localization to SPBs, its ability to ubiquitinate itself or its substrate Sid4, or its mitotic checkpoint function.

Surprisingly, we found that preventing phosphorylation impacted the ability of Dma1 to localize normally to the CR. Though the binding partner(s) of Dma1 at the CR and its potential function there are unknown, our data suggest Dma1 phosphorylation modulates its interaction with the CR during early mitosis. The *dma1-6A* allele may serve as a useful separation of function allele for any future studies addressing this question. It is interesting that Dma1 returns to the division site upon mitotic exit at increased levels compared with early mitosis, and this latter division site localization does not depend on phosphorylation. This suggests that there are two different mechanisms localizing Dma1 to the division site differentially regulated by phosphorylation.

We determined that Dma1 is phosphorylated *in vivo* throughout the cell cycle and that this phosphorylation occurs on six sites. Some of these phosphosites were also identified in global phosphoproteomics screens designed to identify mitotic-specific phosphorylation and two mitotic kinases, Cdk1 and Plo1, phosphorylate Dma1 *in vitro*. It was therefore surprising that we did not detect a significant increase in Dma1 phosphorylation during mitosis nor an effect of eliminating Cdk1 or Plo1 kinase activity on Dma1 phosphostate. While other kinases may act redundantly, considering our data indicates the role of Dma1 phosphorylation is to target it to the CR, we speculate that the kinases responsible for phosphorylating Dma1 *in vivo* may be one of many kinases localized at the cell cortex rather than the SPB.

Phosphorylation of other E3 ubiquitin ligases has been reported to inhibit their E3 ligase activity or switch their substrate preference. As example, IκB kinase phosphorylates the HECT E3 ligase ITCH to inhibit its E3 ligase activity [45] by impairing E2-E3 complex formation [46]. Protein kinase A-dependent phosphorylation of the E3 ligase Smad Ubiquitin Regulatory Factor 1 (Smurf1) changed its affinity for substrates, leading to reduced degradation of one substrate and increased degradation of another substrate [47]. Although our study suggests that dephosphorylation has little effect on Dma1 E3 ubiquitin ligase activity towards its currently known substrates in mitosis, Sid4 and itself, it does not rule out the possibility that Dma1 phosphorylation is important for ubiquitination of its meiotic substrates [48,49] or influence its choice of E2 enzyme partner. Finally, a caveat to our study is that mutations designed to mimic phosphorylation in *dma1-6D/E* may not have done so [50], and thus the effect of constitutive Dma1 phosphorylation may not have been revealed.

## Acknowledgements

The authors thank Drs. Sierra Cullati and Alaina Willet for comments on the manuscript and Dr. Willet for creating the graphical abstract. C.M.J. and A.E.J. were supported by the Cellular, Biochemical, and Molecular Sciences Training Program (NIH T32GM08554). This work was supported by National Institutes of Health grant GM R35131799 to K.L.G. The content is solely the responsibility of the authors and does not necessarily represent the official views of the National Institutes of Health.

## Author contributions

JSC, CMJ, AEJ, KLG conceived the study, KLG supervised the study; JSC, CMJ, MGI, AEJ, KLG designed experiments; JSC, CMJ, MGI, LR, AEJ performed experiments; JSC, CMJ, MGI, LR, AEJ, KLG analyzed data; JSC, CMJ, MGI, KLG wrote the manuscript; JSC, CMJ, MGI, LR, AEJ, KLG made manuscript revisions.

## Data accessibility

The data that support the findings of this study are either in the figures or Supplementary Material of this article or will be made available upon reasonable request of the corresponding author (kathy.gould@vanderbilt.edu).

## References

1 Krapp A and Simanis V (2008) An overview of the fission yeast septation initiation network (SIN). *Biochem Soc Trans* **36**, 411–415.
2 Johnson AE, McCollum D and Gould KL (2012) Polar opposites: fine-tuning cytokinesis through SIN asymmetry. *Cytoskeleton (Hoboken)* **69**, 686–699.
3 Simanis V (2015) Pombe's thirteen – control of fission yeast cell division by the septation initiation network. *J Cell Sci* **128**, 1465–1474.
4 Murone M and Simanis V (1996) The fission yeast dma1 gene is a component of the spindle assembly checkpoint, required to prevent septum formation and premature exit from mitosis if spindle function is compromised. *Embo J* **15**, 6605–6616.
5 Guertin DA, Venkatram S, Gould KL and McCollum D (2002) Dma1 prevents mitotic exit and cytokinesis by inhibiting the septation initiation network (SIN). *Dev Cell* **3**, 779–790.
6 Johnson AE and Gould KL (2011) Dma1 ubiquitinates the SIN scaffold, Sid4, to impede the mitotic localization of Plo1 kinase. *EMBO J* **30**, 341–354.
7 Johnson AE, Collier SE, Ohi MD and Gould KL (2012) Fission yeast Dma1 requires RING domain dimerization for its ubiquitin ligase activity and mitotic checkpoint function. *J Biol Chem* **287**, 25741–25748.
8 Cullati SN and Gould KL (2019) Spatiotemporal regulation of the Dma1-mediated mitotic checkpoint coordinates mitosis with cytokinesis. *Curr Genet* **65**, 663–668.
9 Brooks L 3rd, Heimsath EG Jr, Loring GL and Brenner C (2008) FHA-RING ubiquitin ligases in cell division cycle control. *Cell Mol Life Sci* **65**, 3458–3466.
10 Jones CM, Chen JS, Johnson AE, Elmore ZC, Cullati SN, Beckley JR and Gould KL (2018) Relief of the Dma1-mediated checkpoint requires Dma1 autoubiquitination and dynamic localization. *Mol Biol Cell* **29**, 2176–2189.
11 Chang L and Gould KL (2000) Sid4p is required to localize components of the septation initiation pathway to the spindle pole body in fission yeast. *Proc Natl Acad Sci USA* **97**, 5249–5254.
12 Johnson AE, Chen JS and Gould KL (2013) CK1 is required for a mitotic checkpoint that delays cytokinesis. *Curr Biol* **23**, 1920–1926.
13 Ohkura H, Hagan IM and Glover DM (1995) The conserved *Schizosaccharomyces pombe* kinase plo1, required to form a bipolar spindle, the actin ring, and septum, can drive septum formation in G1 and G2 cells. *Genes Dev* **9**, 1059–1073.
14 Mulvihill DP, Petersen J, Ohkura H, Glover DM and Hagan IM (1999) Plo1 kinase recruitment to the spindle pole body and its role in cell division in *Schizosaccharomyces pombe*. *Mol Biol Cell* **10**, 2771–2785.
15 Tanaka K, Petersen J, MacIver F, Mulvihill DP, Glover DM and Hagan IM (2001) The role of Plo1 kinase in mitotic commitment and septation in *Schizosaccharomyces pombe*. *Embo J* **20**, 1259–1270.
16 Wu JQ, Sirotkin V, Kovar DR, Lord M, Beltzner CC, Kuhn JR and Pollard TD (2006) Assembly of the cytokinetic contractile ring from a broad band of nodes in fission yeast. *J Cell Biol* **174**, 391–402.
17 Chen YH, Wang GY, Hao HC, Chao CJ, Wang Y and Jin QW (2017) Facile manipulation of protein localization in fission yeast through binding of GFP-binding protein to GFP. *J Cell Sci* **130**, 1003–1015.
18 Moreno S, Klar A and Nurse P (1991) Molecular genetic analysis of fission yeast *Schizosaccharomyces pombe*. *Methods Enzymol* **194**, 795–823.
19 Bahler J, Wu JQ, Longtine MS, Shah NG, McKenzie A 3rd, Steever AB, Wach A, Philippsen P and Pringle JR (1998) Heterologous modules for efficient and versatile PCR-based gene targeting in *Schizosaccharomyces pombe*. *Yeast* **14**, 943–951.
20 Wach A, Brachat A, Poehlmann R and Philippsen P (1994) New heterologous modules for classical or PCR-

based gene disruptions in Saccharomyces cerevisiae. *Yeast* **10**, 1793–1808.
21 Elmore ZC, Beckley JR, Chen JS and Gould KL (2014) Histone H2B ubiquitination promotes the function of the anaphase-promoting complex/cyclosome in *Schizosaccharomyces pombe*. *G3* **4**, 1529–1538.
22 Gould KL, Ren L, Feoktistova AS, Jennings JL and Link AJ (2004) Tandem affinity purification and identification of protein complex components. *Methods* **33**, 239–244.
23 Tagwerker C, Flick K, Cui M, Guerrero C, Dou Y, Auer B, Baldi P, Huang L and Kaiser P (2006) A tandem affinity tag for two-step purification under fully denaturing conditions: application in ubiquitin profiling and protein complex identification combined with in vivocross-linking. *Mol Cell Proteomics* **5**, 737–748.
24 McDonald WH, Ohi R, Miyamoto DT, Mitchison TJ and Yates JR III (2002) Comparison of three directly coupled HPLC MS/MS strategies for identification of proteins from complex mixtures: single-dimension LC-MS/MS, 2-phase MudPIT, and 3-phase MudPIT. *Int J Mass Spectrom* **219**, 245–251.
25 Roberts-Galbraith RH, Chen JS, Wang J and Gould KL (2009) The SH3 domains of two PCH family members cooperate in assembly of the Schizosaccharomyces pombe contractile ring. *J Cell Biol* **184**, 113–127.
26 Tabb DL, Fernando CG and Chambers MC (2007) MyriMatch: highly accurate tandem mass spectral peptide identification by multivariate hypergeometric analysis. *J Proteome Res* **6**, 654–661.
27 Ma ZQ, Dasari S, Chambers MC, Litton MD, Sobecki SM, Zimmerman LJ, Halvey PJ, Schilling B, Drake PM, Gibson BW *et al.* (2009) IDPicker 2.0: Improved protein assembly with high discrimination peptide identification filtering. *J Proteome Res* **8**, 3872–3881.
28 McLean JR, Kouranti I and Gould KL (2011) Survey of the phosphorylation status of the Schizosaccharomyces pombe deubiquitinating enzyme (DUB) family. *J Proteome Res* **10**, 1208–1215.
29 Chen JS, Broadus MR, McLean JR, Feoktistova A, Ren L and Gould KL (2013) Comprehensive proteomics analysis reveals new substrates and regulators of the fission yeast clp1/cdc14 phosphatase. *Mol Cell Proteomics* **12**, 1074–1086.
30 Kamps MP and Sefton BM (1989) Acid and base hydrolysis of phosphoproteins bound to immobilon facilitates analysis of phosphoamino acids in gel-fractionated proteins. *Anal Biochem* **176**, 22–27.
31 Boyle WJ, van der Geer P and Hunter T (1991) Phosphopeptide mapping and phosphoamino acid analysis by two- dimensional separation on thin-layer cellulose plates. *Methods Enzymol* **201**, 110–149.
32 Bohnert KA and Gould KL (2011) On the cutting edge: post-translational modifications in cytokinesis. *Trends Cell Biol* **21**, 283–292.
33 Hunter T (2007) The age of crosstalk: phosphorylation, ubiquitination, and beyond. *Mol Cell* **28**, 730–738.
34 Holt LJ (2012) Regulatory modules: coupling protein stability to phosphoregulation during cell division. *FEBS Lett* **586**, 2773–2777.
35 Koch A, Krug K, Pengelley S, Macek B and Hauf S (2011) Mitotic substrates of the kinase aurora with roles in chromatin regulation identified through quantitative phosphoproteomics of fission yeast. *Sci Signal* **4**, rs6.
36 Swaffer MP, Jones AW, Flynn HR, Snijders AP and Nurse P (2018) Quantitative phosphoproteomics reveals the signaling dynamics of cell-cycle kinases in the fission yeast *Schizosaccharomyces pombe*. *Cell Rep* **24**, 503–514.
37 Tay YD, Leda M, Spanos C, Rappsilber J, Goryachev AB and Sawin KE (2019) Fission yeast NDR/LATS kinase Orb6 Regulates exocytosis via phosphorylation of the exocyst complex. *Cell Rep* **26**, 1654–1667 e7.
38 Moreno S and Nurse P (1990) Substrates for p34cdc2: in vivo veritas? *Cell* **61**, 549–551.
39 Songyang Z, Blechner S, Hoagland N, Hoekstra MF, Piwnica-Worms H and Cantley LC (1994) Use of an oriented peptide library to determine the optimal substrates of protein kinases. *Curr Biol* **4**, 973–982.
40 Nakajima H, Toyoshima-Morimoto F, Taniguchi E and Nishida E (2003) Identification of a consensus motif for Plk (Polo-like kinase) phosphorylation reveals Myt1 as a Plk1 substrate. *J Biol Chem* **278**, 25277–25280.
41 Songyang Z, Lu KP, Kwon YT, Tsai LH, Filhol O, Cochet C, Brickey DA, Soderling TR, Bartleson C, Graves DJ *et al.* (1996) A structural basis for substrate specificities of protein Ser/Thr kinases: primary sequence preference of casein kinases I and II, NIMA, phosphorylase kinase, calmodulin-dependent kinase II, CDK5, and Erk1. *Mol Cell Biol* **16**, 6486–6493.
42 Meggio F, Marin O and Pinna LA (1994) Substrate specificity of protein kinase CK2. *Cell Mol Biol Res* **40**, 401–409.
43 Chan KY, Alonso-Nunez M, Grallert A, Tanaka K, Connolly Y, Smith DL and Hagan IM (2017) Dialogue between centrosomal entrance and exit scaffold pathways regulates mitotic commitment. *J Cell Biol* **216**, 2795–2812.
44 Katoh S, Hong C, Tsunoda Y, Murata K, Takai R, Minami E, Yamazaki T and Katoh E (2003) High precision NMR structure and function of the RING-H2 finger domain of EL5, a rice protein whose expression is increased upon exposure to pathogen-derived oligosaccharides. *J Biol Chem* **278**, 15341–15348.
45 Perez JM, Chirieleison SM and Abbott DW (2015) An IkappaB kinase-regulated feedforward circuit prolongs inflammation. *Cell Rep* **12**, 537–544.
46 Perez JM, Chen Y, Xiao TS and Abbott DW (2018) Phosphorylation of the E3 ubiquitin protein ligase

ITCH diminishes binding to its cognate E2 ubiquitin ligase. *J Biol Chem* **293**, 1100–1105.
47 Cheng PL, Lu H, Shelly M, Gao H and Poo MM (2011) Phosphorylation of E3 ligase Smurf1 switches its substrate preference in support of axon development. *Neuron* **69**, 231–243.
48 Krapp A, Del Rosario EC and Simanis V (2010) The role of Schizosaccharomyces pombe dma1 in spore formation during meiosis. *J Cell Sci* **123**, 3284–3293.
49 Krapp A and Simanis V (2014) Dma1-dependent degradation of SIN proteins during meiosis in Schizosaccharomyces pombe. *J Cell Sci* **127**, 3149–3161.
50 Dephoure N, Gould KL, Gygi SP and Kellogg DR (2013) Mapping and analysis of phosphorylation sites: a quick guide for cell biologists. *Mol Biol Cell* **24**, 535–542.

## Supporting information

Additional supporting information may be found online in the Supporting Information section at the end of the article.

**Fig. S1**. Dma1 phosphospectra. Representative mass spectra of phosphopeptides from Dma1 TAPs or HBH purifications are shown. Images were extracted from Scaffold PTM; matched b and y ions are highlighted in red and blue, respectively. Ions resulting from neutral losses are highlighted in green. When available, both MS2 and MS3 (spectrum resulting from further fragmentation of the neutral loss (NL) of the phosphate from the parent ion during MS2 scan) spectra of the same site are shown. Sp/Tp: phosphorylated serine/threonine; Sd/Td: dehydrated serine/threonine (due to neutral loss of phosphate).

**Fig. S2**. Identification of the kinases that phosphorylate Dma1 *in vitro*. (A–C) Recombinant MBP-purified Dma1 proteins were incubated *in vitro* with Cdk1 complex (Cdc2-Cdc13) (A), Plo1 (B), or CK2 (C), resolved by SDS–PAGE, and visualized by Coomassie blue (CB) staining (bottom panels). Labeled proteins were detected by autoradiography (top panels).

**Fig. S3**. (A) Quantification of live whole-cell fluorescence intensity from the indicated strains. $n \geq 41$ non-septated cells. Error bars represent SEM. One-way ANOVA (*dma1* vs. *dma1-6A* $p = 0.10$; *WT* vs. *dma1-6D/E* $p = 0.59$). (B) Quantification of time-lapse imaging of mitotic and cytokinetic events of strains from Fig. 3A–C. See methods for definition of events. n = 11 cells. Error bars represent SEM.